Polymorphisms in fibronectin binding protein A of *Staphylococcus aureus* are associated with infection of cardiovascular devices

Steven K. Lower[a,1,2], Supaporn Lamlertthon[b,c,2,3,4], Nadia N. Casillas-Ituarte[a,1,2], Roberto D. Lins[d,1], Ruchirej Yongsunthon[a,5], Eric S. Taylor[a], Alex C. DiBartola[a], Catherine Edmonson[e], Lauren M. McIntyre[e], L. Barth Reller[b], Yok-Ai Que[f], Robert Ros[g], Brian H. Lower[a], and Vance G. Fowler, Jr.[b,2,3]

[a]Ohio State University, Columbus, OH 43210; [b]Duke University Medical Center, Durham, NC 27705; [c]Naresuan University, Phitsanulok, Thailand 65000; [d]Universidade Federal de Pernambuco, Recife, PE 50670-901, Brazil; [e]University of Florida, Gainesville, FL 32611; [f]University of Lausanne, Lausanne, 1011 Switzerland; and [g]Arizona State University, Tempe, AZ 85287

Edited by Richard P. Novick, New York University School of Medicine, New York, NY, and approved October 5, 2011 (received for review June 8, 2011)

Medical implants, like cardiovascular devices, improve the quality of life for countless individuals but may become infected with bacteria like *Staphylococcus aureus*. Such infections take the form of a biofilm, a structured community of bacterial cells adherent to the surface of a solid substrate. Every biofilm begins with an attractive force or bond between bacterium and substratum. We used atomic force microscopy to probe experimentally forces between a fibronectin-coated surface (i.e., proxy for an implanted cardiac device) and fibronectin-binding receptors on the surface of individual living bacteria from each of 80 clinical isolates of *S. aureus*. These isolates originated from humans with infected cardiac devices (CDI; *n* = 26), uninfected cardiac devices (*n* = 20), and the anterior nares of asymptomatic subjects (*n* = 34). CDI isolates exhibited a distinct binding-force signature and had specific single amino acid polymorphisms in fibronectin-binding protein A corresponding to E652D, H782Q, and K786N. *In silico* molecular dynamics simulations demonstrate that residues D652, Q782, and N786 in fibronectin-binding protein A form extra hydrogen bonds with fibronectin, complementing the higher binding force and energy measured by atomic force microscopy for the CDI isolates. This study is significant, because it links pathogenic bacteria biofilms from the length scale of bonds acting across a nanometer-scale space to the clinical presentation of disease at the human dimension.

adhesion | binding strength | host–pathogen interaction | pacemaker | prosthesis

The Gram-positive bacterium *Staphylococcus aureus* colonizes the anterior nares (1, 2) of 2 billion individuals worldwide (3). If *S. aureus* enters the bloodstream, it can cause an infection in the form of a biofilm living on the surface of an implanted medical device. This possibility is particularly important with cardiac devices, for which rates of infection have increased exponentially over the last decade (4). Because cardiac device infections (CDIs) are difficult or impossible to eradicate with antibiotic therapy alone (5, 6), standard practice is complete removal of the infected generator and endovascular leads.

The underlying pathogenesis of *S. aureus* CDI is the ability of the organism to produce a biofilm (Fig. 1*A*). During the early stage of infection *S. aureus* expresses cell-wall proteins that serve to initiate a biofilm by aiding in the initial attachment and colonization of host tissues or devices (7). These covalently anchored transmembrane proteins are designated "microbial-surface components recognizing adhesive matrix molecules" (MSCRAMMs) (8) because they bind to human proteins such as fibronectin (Fn) or fibrinogen commonly found in the bloodstream (9). Implanted materials such as endovascular prostheses become coated with these host proteins (10). Fn is the host protein most commonly encountered on long-term prostheses (10, 11).

The MSCRAMM Fn-binding protein (FnBP) plays a central role in the pathogenesis of *S. aureus* infections (12, 13) by facilitating binding of bacteria to host Fn. Recent studies show Fn-binding protein A (FnBPA) from the type-strain of *S. aureus* binds to human Fn through a tandem β-zipper mechanism (14, 15). However, little is known about the clinical significance of this binding event. Herein, we probe the binding mechanism between Fn on a substrate (i.e., a proxy for a prosthesis) and Fn-binding protein on *S. aureus* (Fig. 1*B*) through a complementary experimental and theoretical approach that includes (*i*) atomic force microscopy (AFM) measurements of binding forces on 80 different clinical isolates of *S. aureus* obtained from humans with or without cardiac device implants; (*ii*) sequence data for *fnbA* (the gene for FnBPA) from the same clinical isolates; and (*iii*) molecular dynamics (MD) simulations of binding reactions between Fn and FnBPA.

Results and Discussion

Binding Forces on Clinical Isolates of *S. aureus*. The binding forces that initiate a biofilm have been investigated for a handful of type-strains or laboratory-derived strains of *S. aureus* (e.g., refs. 16–20) and related species such as *Staphylococcus epidermidis* (e.g., ref. 21). However, no one has examined a large population of clinically derived strains of *Staphylococcus* that cause disease in humans. For this study, we used 80 different *S. aureus* isolates from three distinct clinical groupings (Table S1): (*i*) patients with *S. aureus* bacteremia (i.e., *S. aureus* in the bloodstream) and confirmed CDI ($n = 26$); (*ii*) patients with *S. aureus* bacteremia and an uninfected cardiac device (CDU; $n = 20$); and (*iii*) the nares of healthy subjects living in the same medical referral area (HS; $n = 34$).

AFM was performed on at least 10 living cells for each isolate, generating >250,000 force curves. Attractive interactions resulted

Author contributions: S.K.L. and V.G.F. designed research; S.K.L., S.L., N.N.C.-I., R.D.L., R.Y., E.S.T., A.C.D., B.H.L., and V.G.F. performed research; C.E., L.M.M., L.B.R., Y.-A.Q., and R.R. contributed new reagents/analytic tools; S.K.L., S.L., N.N.C.-I., R.D.L., L.M.M., and V.G.F. analyzed data; and S.K.L., N.N.C.-I., R.D.L., and V.G.F. wrote the paper.

V.G.F. has served as a consultant for Astellas, Cubist, Inhibitex, Merck, Johnson & Johnson, Leo Pharmaceuticals, NovaDigm, The Medicines Company, Baxter Pharmaceuticals, and Biosynexus; has received grant or research support from Astellas, Cubist, Merck, Theravance, Cerexa, Pfizer, Novartis, and Advanced Liquid Logic; has received honoraria from Arpida, Astellas, Cubist, Inhibitex, Merck, Pfizer, Targanta, Theravance, Wyeth, Ortho-McNeil, Novartis, and Vertex Pharmaceuticals; and has served as a member of the advisory committee and on the speakers' bureau for Cubist. All other authors: no conflicts.

This article is a PNAS Direct Submission.

Data deposition: The sequences reported in this paper have been deposited in GenBank data (accession nos. JF809617 to JF809662, and JN848717 to JN848750).

[1]S.K.L., N.N.C.-I., and R.D.L. contributed equally to this work.

[2]To whom correspondence may be addressed: E-mail: lower.9@osu.edu, supapornl@nu.ac.th, casillas-ituarte.1@osu.edu, or vance.fowler@duke.edu.

[3]S.L. and V.G.F. contributed equally to this work.

[4]Present address: Naresuan University, Phitsanulok, Thailand 65000.

[5]Present address: Corning Inc., Corning, NY 14831.

This article contains supporting information online at www.pnas.org/lookup/suppl/doi:10.1073/pnas.1109071108/-/DCSupplemental.

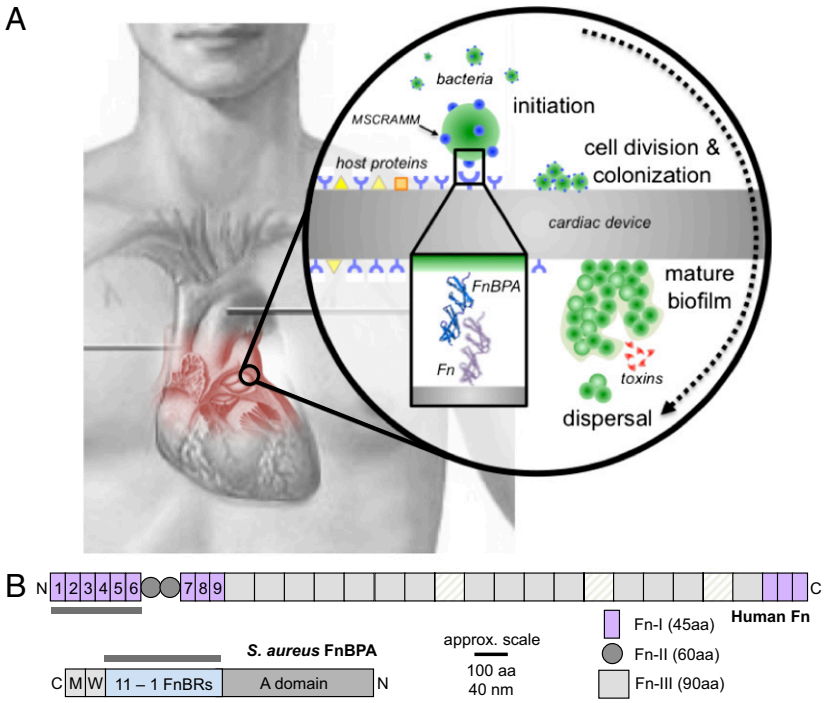

C

1	~~GPIIQNNKFEYKEDTIKETLTGQYDKNLVTTVEEEYDSS	550
2	~~~~~~~~~~TLDIDYHTAIDGGGGYVD~~GYIETIEETDSS	580
3	~~~~~~~~~~AIDIDYHTAVDSEAGHVG~~GYTESSEESNP	609
4	~~~~~~~~~~IDF~EESTHENSKHHA~~~DVVEYEEDTNPG	636
5	GGQVTTESNLVEFDEESTKGIVTGAV~~~SDHTTVEDTK	672
6	~~EYTTESNLIELVDELPEEHGQ~~~~~~AQGPVEEITK	703
7	NNHHISHS~~~~~~~~~~GLGTENGH~~~GNYDVIEEIEENS	732
8	~~~~~~~~~~HVDIKSEL~GYEGGQNS~~~GNQSFEEDTEEDKP	762
9	KYEQGGN~~IVDIDFDSVPQIHGQNK~~~GNQSFEEDTEKDKP	800
10	KYEHGGN~~IIDIDFDSVPHIHGFNK~~~HTEIIEEDTNKDKP	838
11	SYQFGGH~NSVDFEEDTLPKVSGQNE~~~GQQTIEEDTTP	874

Fig 1. (*A*) Stages of a *Staphylococcus aureus* biofilm on a cardiac prosthesis: initiation, colonization, maturation, and dispersal. The infection is triggered by a bond between host proteins such as Fn that coat the device and bacterial proteins such as Fn-binding protein A (FnBPA). FnBPA, or other MSCRAMMs (8) are expressed on the exterior cell wall during the early stages of infection. Extracellular toxins are produced as the biofilm matures (7). (*B*) Structure of Fn and FnBPA highlighting the binding regions (gray lines). Binding sites in Fn are the string of F1 modules at the N terminus (50), whereas FnBPA binds through a series of 11 FnBRs, each ~40 residues (14, 15). (*C*) Amino acid sequence of the 11 FnBRs in FnBPA from the type-strain of *S. aureus* (NCTC 8325). Red letters highlight locations of polymorphisms identified by sequencing *fnbA* in clinical isolates of *S. aureus*.

in distinct, nonlinear profiles as the Fn-probe was pulled from contact with a bacterium (Fig. 2*A*). This sawtooth-shaped feature was observed when an Fn-tip was used to probe a strain of *Lactococcus lactis* (a Gram-positive bacterium whose native genome lacks MSCRAMMs) engineered to express only FnBPA or Fn-binding protein B (FnBPB) on its cell wall (20). Therefore, these signatures likely originate from the mechanical unfolding of proteins, in this case the sequential unraveling of domains within the complex of Fn bound to FnBP on *S. aureus* (see the worm-like chain model in Fig. 2*A*).

Recent NMR and X-ray crystallography studies have revealed 11 domains (~40 residues each) within FnBPA capable of forming tandem β-zipper interactions with F1 domains in Fn (Fig. 1*C*) (14, 15). *S. aureus* FnBPB, which has sequence homology with FnBPA, has 10 of these Fn-binding repeats (FnBRs) (22). These NMR and crystallography studies were conducted with small purified or synthetic fragments of Fn and FnBPA (14, 15). The force measurements presented herein complement that work by probing the binding complex on living *S. aureus* expressing intact proteins in their native state. Force profiles like those in Fig. 2*A* show a structurally functional protein–protein binding complex that can be unfolded mechanically with an external force.

The binding activity for each isolate was defined as the frequency of observing a discrete sawtooth-shaped force signature. Fig. 2*B* shows the distribution of binding-force signatures for bacteria from each of the three clinical sources of *S. aureus*. The average binding activity of the CDI isolates was significantly greater than that of the CDU and HS populations ($P < 0.05$). This difference in binding suggests that a microorganism's "force taxonomy" could serve as an indicator of pathogen-related risk for patients. This type of screening could be helpful, given that >80% of health care-associated *S. aureus* infections come from endogenous sources (23).

Single Amino Acid Polymorphisms in FnBPA from *S. aureus*. Why do bacteria from different clinical groups exhibit different bond activity when all measurements were performed on isolates of the same bacterial species expressing the same FnBP? To address this question, the sequence variation in FnBPA was determined by sequencing the portion of *fnbA* that codes for the 11 FnBRs. We chose to focus on *fnbA* rather than *fnbB* because all isolates had *fnbA*, but only 85% of the CDI isolates possessed the gene for FnBPB (i.e., 15% of the CDI isolates had only *fnbA*). This distribution is similar to that reported in other studies of clinical isolates, which have found that >70% of isolates have both FnBPA and FnBPB, 20% have only FnBPA, but isolates encoding only FnBPB are rare (~1%) (24, 25).

Fig. 1*C* shows the primary sequence of FnBPA from the type-strain *S. aureus* NCTC 8325 (26) and the location of six non-synonymous SNPs that were found in FnBPA from our clinical

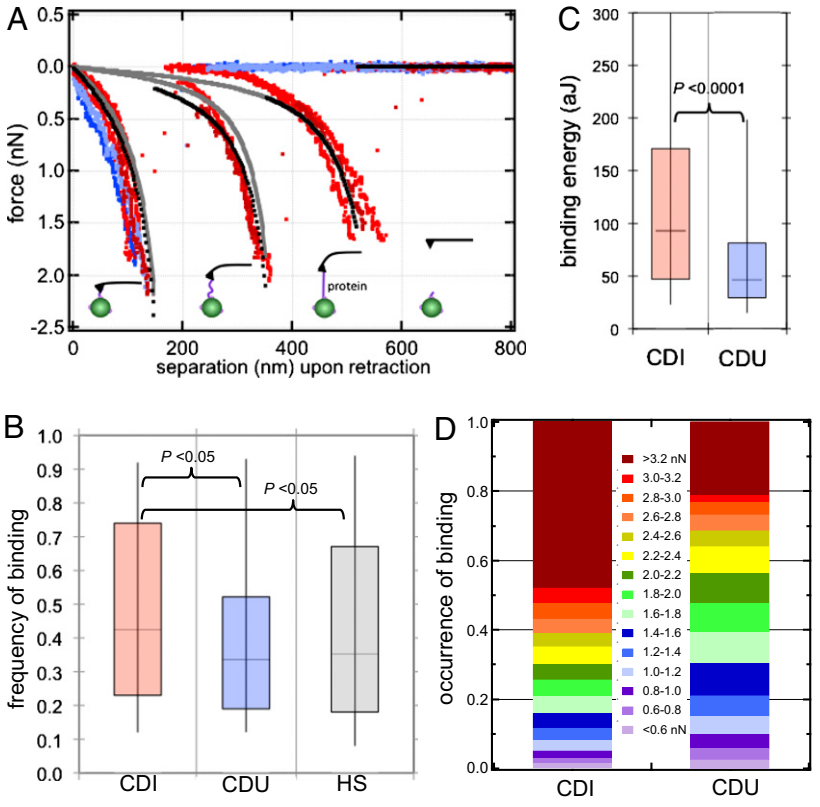

Fig 2. (*A*) Experimentally measured force of bonds that form between an Fn-coated substrate and Fn-binding proteins expressed on individual, living bacteria immersed in buffer. Shown are spectra from some of the 80 different clinical isolates of *S. aureus* (CDI, red; CDU, blue). Gray curves are theoretical profiles predicted by the worm-like chain (WLC) model: $F(x) = (k_B T/p)\,(0.25\,(1 - x/L)^{-2} + (x/L) - 0.25)$; where F is force, x is the extension distance, k_B is Boltzmann's constant (1.381×10^{-23} J K^{-1}), T is temperature (kelvin), L is the contour length of the extended proteins, and p is the persistence length (0.04 nm corresponding to 10 molecules of Fn and FnBPA bound in parallel; see ref. 51). The black curve is the summation of the three individual WLC profiles. (*B*) Box and whisker plot of binding activity (frequency of a sawtooth force signature) for isolates from the CDI (n = 26), CDU (n = 20), and HS (n = 34) groups. (*C*) Box and whisker plot of the binding energy (in aJ; 10^{-18} J) for the CDI and CDU groups. Energies were calculated by integrating force with respect to distance (Fig. S2). Whisker ends represent ninth and 91st percentiles. (*D*) Distribution of binding forces (in nN) for an Fn-coated substrate on isolates from the CDI and CDU groups.

isolates. Three SNPs corresponding to residues E652D, H782Q, and K786N in FnBPA were significantly more common in the CDI isolates ($P < 0.01$) (Table 1). For these three SNPs, the occurrence of multiple (i.e., two or three) polymorphisms in the same *S. aureus* isolate also was more common for the CDI group ($P < 0.01$) (Table S2). All three of these polymorphisms are located within regions of FnBPA identified as high-affinity FnBRs (22). This association between CDI and the presence of the three SNPs was not explained by bacterial ancestry as assessed by multilocus sequence typing (MLST) (Table S3), by the presence of other MSCRAMM adhesins including bone sialoprotein-binding protein (*bbp*), clumping factor A (*clfA*), clumping factor B (*clfB*), collagen-binding adhesion (*cna*), elastin-binding protein (*ebpS*), extracellular fibrinogen-binding protein (*efb*), polysaccharide intercellular adhesin (*icaA*), or major histocompatibility analog protein/extracellular adherence protein (*map*/*eap*) (Table S4), or by the overexpression of *fnbA* (Fig. S1).

Binding Energy on Clinical Isolates of *S. aureus*. Fig. 2*B* shows higher binding activity for the CDI isolates. The results in Table 1 reveal nonsynonymous SNPs (positions 652, 782, and 786 in FnBPA) that are significantly more common in the CDI group than in the two other clinical groups. To determine whether there also is a stronger bond for the CDI isolates, the energy (or work) of binding for each force curve was determined by integrating force with respect to distance (Fig. S2). *S. aureus* isolates from the CDI group exhibited stronger binding energy ($P < 0.01$) (Fig. 2*C* and Fig. S3). The binding force also was stronger for the CDI group ($P < 0.01$) (Fig. 2*D*).

Next, we evaluated potential associations between binding strength and the presence of FnBPA polymorphisms. Regardless of clinical origin (i.e., CDI, CDU, or HS), isolates with two or three SNPs exhibited significantly higher binding energies than isolates with no or one SNP at positions 652, 782, and/or 786 in FnBPA (Table 2). This relationship between binding and the presence of

Table 1. SNPs found in the 11 Fn-binding repeats within *fnb*A and the corresponding alteration to FnBPA

Nonsynonymous SNP	Position in *fnbA*	Amino acid change in FnBPA	% (number) of nonsynonymous SNPs			*P* value	
			CDI n = 26	CDU n = 20	HS* n = 34	CDI vs. CDU	CDU vs. HS
GAG to GAT	2073	E652D	46% (12)	5% (1)	12% (4)	0.0021†	0.41
CAT to CAA	2463	H782Q	54% (14)	5% (1)	9% (3)	0.0005‡	0.60
AAA to AAT	2475	K786N	54% (14)	15% (3)	35% (12)	0.0068†	0.11
CAC to CAA	2577	H818Q	12% (3)	20% (4)	9% (3)	0.43	0.24
ACT to AAT	2595	T826N	0	20% (4)	12% (4)	0.0170§	0.41
AGT to AAT	2633	S839N	69% (18)	50% (10)	32% (11)	0.19	0.20

Reported are the percentages (and numbers) of isolates from patients with CDI, CDU, and the anterior nares of HS. *S. aureus* 8325–4 served as the reference strain. The difference between groups was tested for CDI vs. CDU as well as a comparison of the two control groups (CDU vs. HS). All *P* values were calculated with the χ^2 test. The significance of *P* values was confirmed with Fisher's Exact test.

*One isolate from the healthy subjects had a double-nucleotide polymorphism at position 2099 and 2100 in *fnbA* (GCA to GTG) resulting in A661V in FnBPA.

†$P < 0.01$.

‡$P < 0.001$.

§$P < 0.05$.

Table 2. Binding energy (work) as a function of the occurrence of polymorphisms in the amino acid sequence of FnBPA in *S. aureus*

Occurrence of SNPs in FnBPA	Binding energy		*P* value
	Low (<74 aJ)	High (>74 aJ)	
CDI and CDU			
≤1 SNP at 652, 782, 786	20	10	<0.01
>1 SNP at 652, 782, 786	3	13	
CDI, CDU, and HS			
≤1 SNP at 652, 782, 786	34	25	<0.05
>1 SNP at 652, 782, 786	6	15	

Binding energy was determined by integrating the measured force profiles (see Fig. S2 for reference) obtained on isolates from patients with infected (CDI) or uninfected (CDU) cardiovascular implants, as well as nasal carriage isolates from healthy subjects (HS). $P = 0.0045$ for CDI and CDU isolates ($n = 46$), two-tailed Fisher's exact test; $P = 0.0020$, χ^2 test. When HS isolates are included ($n = 80$), the two-tailed $P = 0.0406$ for Fisher's exact test, and $P = 0.0222$ for the χ^2 test.

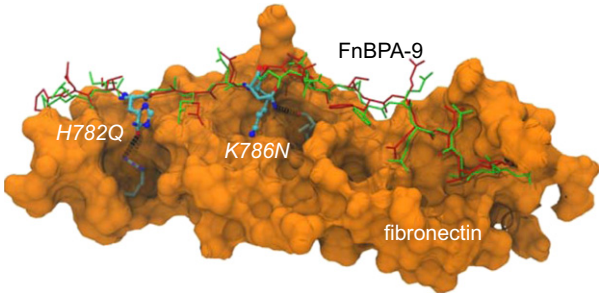

Fig. 3. MD simulations of Fn (orange surface) bound to wild-type FnBPA-9 (red stick model) vs. a variant of FnBPA-9 with the substitutions H782Q and K786N (green sticks). Two extra hydrogen bonds at positions Q782 and N786 in FnBPA are highlighted as dotted black lines/rings. No significant hydrogen-bond activity was detected at either of these two positions for the native sequence of FnBPA. Atoms are shown for both Fn and the FnBPA-9 variant [Q/N in the Corey–Pauling–Koltun (CPK) model and His (H)/K in the stick model]. Atoms are color-coded: carbon, cyan; nitrogen, blue; and oxygen, red. Hydrogen atoms have been removed for clarity.

these three polymorphisms also was tested with a photometric adhesion assay. This assay showed an increased number of *S. aureus* cells on Fn-coated substrates for isolates that have polymorphisms E652D, H782Q, and/or K786N in FnBPA (Fig. S4). Taken together, these experiments demonstrate a significant relationship between the sequence of FnBPA and the actual activity of this protein in its native state within a living cell.

MD Simulations of Fn Binding to FnBPA. MD simulations were used to determine whether the three SNPs influence the structure of the Fn–FnBPA binding mechanism. MD simulations were performed comparing Fn interactions in the wild-type FnBPA-9 and in FnBPA-9 with SNPs H782Q, and K786N as well as in FnBPA-5 containing either E or D at position 652 (Fig. 1 *B* and *C*). Fig. 3 shows the final structures of 10-ns MD simulations for both wild-type and variant FnBPA-9 in complex with Fn. The simulations show that Q782 and N786 are able to form well-defined, stable, extra hydrogen bonds with Fns R125 and I106, respectively (see the two dotted lines in Fig. 3 and Movie S1). In the case of H782Q, the hydrogen bond is possible only with Gln (Q), because of its hydrogen-binding acceptor site. The hydrogen bond involves the side chains of FnBPA-9 Q782 and Fn R125. Over the course of the simulation, hydrogen bonds between Gln-782 and Arg-125 were observed 43% of the sampled time. In the case of K786N in FnBPA, both have a donor site, but Lys (K) has a longer chain than Asn (N) and does not fit well in the small cavity. Therefore, the hydrogen bond is predicted between the side chain of FnBPA N786 and the backbone of Fn I106. Over the course of the simulation, hydrogen bonds between Asn-786 and Ile-106 were observed 86% of the sampled time. Although a carboxyl group is largely conserved at position 652 of FnBPA-5, MD simulations of this candidate SNP reveal that D in this sequence is capable of forming a higher number of hydrogen bonds with Fn than E at the same position (average number of hydrogen bonds was 0.75 for D and 0.35 for E; Fig. S5 and Movie S2).

While the contribution of a single hydrogen bond per se may not be sufficient to generate the increased binding energy (27, 28), each FnBPA molecule in *S. aureus* has the capacity to bind up to nine molecules of Fn (29, 30), and each *S. aureus* bacterium expresses multiple copies of FnBPA on its cell wall. Experimental measurements on biomolecular association have indicated that an individual uncharged hydrogen bond contributes *ca*. 0.5–1.5 kcal/mol to binding energy, increasing specificity by two- to 20-fold (31, 32). These values reach up to 4 kcal/mol if a charged group is involved, increasing specificity by a factor of 1,000. Thus, hydrogen bonds provide specificity as well as indirect stability at protein–protein interfaces (33, 34). In addition, unfavorable steric interactions, such as exposed surface area or unpaired charged donors or acceptors, can yield far higher specificity. Therefore, additional hydrogen bonds can lead to a larger protein–protein contact area, resulting in stronger bonds between the molecules (35, 36). Indeed, X-ray crystallographic measurements have shown that interactions between F1 domains in Fn and FnBRs in FnBPA bury significant amounts of surface area, thereby enhancing the efficiency of this protein–protein interaction (15).

Binding Forces of Synthetic FnBR-9 Peptides. A final experimental test was performed to determine whether these polymorphisms could be responsible for the increased binding demonstrated by the MD simulations. AFM was used to probe directly the strength of the bond between Fn and synthesized peptides that were identical to the $^{2-3}$F1 binding motif in FnBR-9, a repeat that contains two of the three key polymorphisms (H782Q and K786N) (Fig. 1*C*). Compared with the wild-type sequence, the activity (or frequency) of binding was 15 and 34% higher for peptides with the single and double polymorphisms, respectively (Table 3). The avidity of bonds, as measured by force and energy, also was stronger for the single and double polymorphisms than for the wild-type peptide. Statistically, the double mutant has a greater impact on the binding complex (see *P* values in Table 3). This experimental evidence shows that our identified polymorphisms H782Q and K786N could indeed be responsible for the increased binding observed for *S. aureus* with this variant FnBPA.

Limitations of the Present Study. The work presented here shows a link between FnBPA in *S. aureus* and the outcome of bacteremic patients with cardiac device implants. However, other *S. aureus* adhesins, such as those shown in Table S4, also could play an important role in the pathogenesis of disease on cardiac devices or other surgical implants. For example, there is a great deal of sequence homology between FnBPA and FnBPB (22). Although Shinji et al. (25) show that FnBPA is more important for in vitro and in vivo infections by *S. aureus*, these authors note, "cooperation between FnBPA and FnBPB is indispensable." For the 15% of the CDI isolates that lacked *fnbB* in our study (Table S4), every one expressed a variant of FnBPA with at least two of the three polymorphisms (E652D, H782Q, and/or K786N), and 75% of the *fnbB*-deficient CDI isolates exhibited strong (i.e., higher than the median) binding to Fn as measured by AFM.

The association between the clinical origin of *S. aureus* (e.g., CDI) and specific SNPs in FnBPA leads to another important, unresolved question. Were these polymorphisms present before CDI, or did they arise as a consequence of it? The latter is conceivable, given that virulence genes like *fnbA* can undergo rela-

Table 3. Experimentally measured binding reactions between Fn and three synthetic peptides

Peptide ID	Amino acid sequence*	Binding to Fn		
		Frequency	Force (pN)	Energy (aJ)
1	VPQIHGQNKGNQSFEEDTEC†	0.59 ± 0.06	231 ± 17	1.51 ± 0.28
2	VPQI**Q**GQNKGNQSFEEDTEC	0.68 ± 0.07 $P = 0.092$	298 ± 26 $P < 0.0001$****	1.90 ± 0.58 $P = 0.23$
3	VPQI**Q**GQN**N**GNQSFEEDTEC	0.79 ± 0.07 $P = 0.002$**	352 ± 30 $P < 0.0001$****	3.67 ± 0.48 $P < 0.0001$****

Peptide 1 is identical to the wild-type sequence of $^{2\text{-}3}$F1-binding motifs in FnBR-9 (22). Bold, underlined letters show single or double polymorphisms (Q and N) in the other two peptides. For each peptide, two different peptide-coated tips were used in force measurements. Reported values are the average ± 95% confidence interval. *P* values were calculated with a *t* test for 1 vs. 2 and 1 vs. 3. **$P < 0.01$; ****$P < 0.0001$. pN, picoNewtons.

*A cysteine residue (C) was added to the C terminus so that each peptide could be linked to a gold-coated atomic force microscope tip through the thiol group.

†Residues V through E represent the primary sequence of amino acids 778–796 in FnBR-9 of FnBPA from the type-strain *S. aureus* 8325.

tively rapid molecular evolution, compared with housekeeping genes, in populations of *S. aureus* (e.g., see ref. 37). Because endogenous sources, typically colonies in the nasal mucosa, cause >80% of *S. aureus* infection (1, 23), the differences in *fnbA* between the HS and CDI groups (Table 1 and Table S2) could suggest that the polymorphisms arise in the setting of infection. One the other hand, some isolates from the HS and CDU groups (5–27%) have one or two of the three key SNPs (Table S2). These SNPs also are found in a range of MLST backgrounds (Table S3). This observation suggests that the population of isolates that are present in the community is responsible for infections and that an infection with an isolate that has these three polymorphisms increases the likelihood that the device itself will become infected. This observation also would mean that individuals colonized with *S. aureus* isolates lacking the three polymorphisms actually could have a lower risk of serious device-related infection.

This important question could be resolved by comparing *fnbA* sequences from CDI isolates and nasal carriage isolates from the same patients collected before and after infection. Unfortunately, it is not standard practice to collect nasal carriage specimens at the time of implantation or initial presentation of disease. Regardless of the origin, our discovery of an association between specific SNPs and clinical severity of inflection implies that specific polymorphisms in the FnBRs of FnBPA influence the likelihood of CDI in patients with *S. aureus* bacteremia.

Implanted medical devices improve the lives of countless patients. Ironically, these same devices place some patients at risk for device-associated infections. Although *S. aureus* is the leading cause of prosthetic valve endocarditis (38), not all patients with *S. aureus* in their blood (i.e., bacteremia) develop an infected device. Whether a patient develops an infection probably depends on attributes of both the human host (e.g., physical health) and the bacteria pathogen. This article touches on the pathogen-related risk by demonstrating an important link from the bedside to the bond, i.e., the clinical presentation of disease at the human dimension and the nanometer-scale force that triggers a biofilm. Our experimental measurements and theoretical simulations show that polymorphisms in key binding proteins lead to stronger, more resilient binding mechanisms that select for isolates of *S. aureus* that form infectious biofilms on cardiovascular devices in humans. Perhaps, additional work will reveal a fundamental force law that can be exploited to prevent *S. aureus* from forming the initiating bond in the first place.

Materials and Methods

Blind experimental practices were performed to the extent possible. *S. aureus* isolates were collected from 80 different humans (Table S1) and assigned a unique study number. Importantly, we used a rigorous study design to minimize potential for bias. For example, investigators assembling AFM measurements and investigators ascertaining clinical cases and generating *fnbA* sequence data were fully blinded to the results of the other team. MD simulations were performed by an individual who was unaware of case ascertainment, AFM analyses, or *fnbA* sequencing. Further details are given in *SI Materials and Methods*.

Source of *S. aureus* Isolates Used in Experiments. Bacterial isolates originated from the *S. aureus* bacteremia registry at Duke University Medical Center. CDI isolates ($n = 26$) came from patients with confirmed infection of a cardiac prosthesis (e.g., permanent pacemaker, implantable cardioverter defibrillator, or prosthetic cardiac valve). A device was confirmed microbiologically as infected if cultures from the prosthetic device, generator pocket, or electrode lead yielded *S. aureus*. CDI was confirmed clinically as infected if echocardiography demonstrated valvular or lead vegetations or the modified Duke criteria for definite infective endocarditis were met (39). CDU isolates ($n = 20$) were obtained from the bloodstream of patients with uninfected prosthetic devices. A device was defined as uninfected if the patient had no evidence of device infection at the time of the initial blood culture, the cardiac device was not removed, and there was no evidence of recurrent infection 12 wk after the onset of bacteremia (i.e., no *S. aureus* in the bloodstream) or no evidence of device infection at autopsy. To account for geographic variation of strains, the HS population of *S. aureus* came from the anterior nares of asymptomatically colonized subjects ($n = 34$) living in the same medical referral area.

AFM Experiments with Clinical Isolates of *S. aureus* and Peptides. Each *S. aureus* isolate was cultured in tryptic soy broth to exponential stage ($OD_{600} = 0.51 \pm 0.01$) so that they expressed FnBPA on their exterior surface (7, 20). Washed cells were deposited onto Fn-coated slides (BD Biosciences). An inverted optical microscope (Axiovert 200M; Zeiss) was used to position a Fn-coated tip (nominal radius 20 nm, measured spring constant 0.1 ± 0.06 nN nm^{-1}) over a *S. aureus* bacterium within the AFM (Veeco Bioscope AFM with Nanoscope IV controller). Forces were measured on live cells immersed in PBS (pH 7.4) according to procedures given in refs. 20 and 40. The tip was pressed against a cell until the cantilever flexed 100 nm. A single approach–retraction cycle took 1–2 s. The vertical travel of the *z*-piezoelectric scanner was 2.7 μm. Data acquisition was confined to <30 min from harvesting to assure cell viability (40).

Synthetic peptides (United Biosystems) were sequenced with MS to confirm sequence identity and analyzed with HPLC to ensure >95% purity. Each peptide was linked to an AFM tip through a strong, covalent bond between the gold on the tip and the thiol group of a cysteine engineered at the C terminus of each peptide (41). AFM measurements were performed in PBS with both commercially available Fn-coated slides (BD-Biosciences) and homemade slides coated with 0.1% Fn-solution. Control experiments were performed with uncoated AFM tips on Fn-coated slides in PBS.

Amino Acid Polymorphisms in FnBPA from Clinical Isolates of *S. aureus*. Genomic DNA was extracted from *S. aureus* cultures using the Ultraclean Microbial DNA Isolation Kit (MO BIO). The *fnbA* gene was amplified by primer *fnbA*-F and *fnbA*-R (Table S5) for use as the sequencing template. PCR products then were sequenced in both directions to cover the entire Fn-binding region corresponding to amino acids 512–874 in *S. aureus* FnBPA. The length of the translated FnBPA was the same in all isolates, 363 residues. Each isolate's sequence was compared with *fnbA* from reference strain *S. aureus* NCTC 8325 (UniProt accession number P14738) (26) using the ClustalW and DNASTAR programs. The *fnbA* sequences reported in this paper have been deposited in GenBank data (accession no. JF809617–JF809662, and JN848717–JN848750).

MD Simulations of Fn Interactions with FnBPA. MD simulations were performed by starting with coordinates for Fn–FnBPA complexes determined by X-ray crystallography (15). The $^{4\text{-}5}$F1:FnBPA-5 complex [Protein Data Bank (PDB) ID code 2RL0] was used for the simulations of FnBPA-5 containing either D or E at position 652. The FnBPA-9 3D structure was obtained by replacement of the FnBPA-5 sequence in the Fn-FnBPA-5 complex ($^{2\text{-}3}$F1:FnBPA-5; PDB ID code

3CAL) and was used as a starting point for the simulations of H782Q and/or K786N. The replacement of sequence FnBPA-5 and -9 is a reasonable change, given that FnBPA has multiple high-affinity binding repeats for the same Fn scaffold and protein structure is more evolutionarily conserved than sequence (42). Indeed, the crystal structures reveal remarkable similarity in the binding motifs between $^{4}F1^{5}F1$/STAFF1, $^{4}F1^{5}F1$/STAFF5, $^{2}F1^{3}F1$/STATT1, and $^{2}F1^{3}F1$/STATT5 (15).

Residue replacement was carried out with DeepView software (43). pK_a calculations were performed with PROPKA (44) to evaluate protonation states of each titratable residue. The systems were solvated in explicit water using the simple point charge (SPC) model (45); counter ions were added as necessary to ensure system neutrality, and geometry was optimized using 1,000 steps of the steepest descent algorithm. For each system, a 10-ns MD simulation was performed at the isothermal isobaric (NPT; N, moles; P, pressure; T, temperature) ensemble using the double-precision parallel version of the GROMACS 4 (46). Temperature was kept at 300 K using the Nosé–Hoover thermostat (47), and pressure was maintained at 1 bar via the Parrinello–Rahman method (48). Periodic boundary conditions were used with a 1.4-nm cutoff for nonbonded interactions. Long-range electrostatic corrections were taken into account by the particle mesh Ewald method (49).

ACKNOWLEDGMENTS. T. J. Beveridge, J. Tak, the PNAS editor, and two anonymous reviewers provided constructive comments. This work was supported by Grants R21HL086593, R01AI068804, and K24AI093969 from the National Institutes of Health and by Grant EAR0745808 from the National Science Foundation. R.D.L. was supported by Grants from Brazilian National Council for Scientific and Technological Development (CNPq), The State of Pernambuco Science Foundation (FACEPE), and the Brazilian National Science and Technology Institute for Integrated Markers (INCT-INAMI). Y.A.Q. was supported by Grant PASMP3-123226 from the Swiss National Science Foundation/Swiss Medical Association and SICPA.

1. von Eiff C, Becker K, Machka K, Stammer H, Peters G; Study Group (2001) Nasal carriage as a source of *Staphylococcus aureus* bacteremia. *N Engl J Med* 344:11–16.
2. Foster TJ (2004) Nasal colonization by *Staphylococcus aureus*. *Nat Med* 10:447.
3. Richardson AR, Libby SJ, Fang FC (2008) A nitric oxide-inducible lactate dehydrogenase enables *Staphylococcus aureus* to resist innate immunity. *Science* 319: 1672–1676.
4. Greenspon AJ, et al. (2011) 16-year trends in the infection burden for pacemakers and implantable cardioverter-defibrillators in the United States 1993 to 2008. *J Am Coll Cardiol* 58:1001–1006.
5. Klevens RM, et al.; Active Bacterial Core surveillance (ABCs) MRSA Investigators (2007) Invasive methicillin-resistant *Staphylococcus aureus* infections in the United States. *JAMA* 298:1763–1771.
6. Stewart PS, Costerton JW (2001) Antibiotic resistance of bacteria in biofilms. *Lancet* 358:135–138.
7. Lowy FD (1998) *Staphylococcus aureus* infections. *N Engl J Med* 339:520–532.
8. Patti JM, Allen BL, McGavin MJ, Höök M (1994) MSCRAMM-mediated adherence of microorganisms to host tissues. *Annu Rev Microbiol* 48:585–617.
9. Proctor RA, Mosher DF, Olbrantz PJ (1982) Fibronectin binding to *Staphylococcus aureus*. *J Biol Chem* 257:14788–14794.
10. Darouiche RO (2004) Treatment of infections associated with surgical implants. *N Engl J Med* 350:1422–1429.
11. Arrecubieta C, et al. (2006) The role of *Staphylococcus aureus* adhesins in the pathogenesis of ventricular assist device-related infections. *J Infect Dis* 193:1109–1119.
12. Que YA, et al. (2005) Fibrinogen and fibronectin binding cooperate for valve infection and invasion in *Staphylococcus aureus* experimental endocarditis. *J Exp Med* 201:1627–1635.
13. Piroth L, et al. (2008) The fibrinogen- and fibronectin-binding domains of *Staphylococcus aureus* fibronectin-binding protein A synergistically promote endothelial invasion and experimental endocarditis. *Infect Immun* 76:3824–3831.
14. Schwarz-Linek U, et al. (2003) Pathogenic bacteria attach to human fibronectin through a tandem beta-zipper. *Nature* 423:177–181.
15. Bingham RJ, et al. (2008) Crystal structures of fibronectin-binding sites from *Staphylococcus aureus* FnBPA in complex with fibronectin domains. *Proc Natl Acad Sci USA* 105:12254–12258.
16. Simpson KH, Bowden G, Höök M, Anvari B (2003) Measurement of adhesive forces between individual Staphylococcus aureus MSCRAMMs and protein-coated surfaces by use of optical tweezers. *J Bacteriol* 185:2031–2035.
17. Mitchell G, et al. (2008) Staphylococcus aureus SigB activity promotes a strong fibronectin-bacterium interaction which may sustain host tissue colonization by small-colony variants isolated from cystic fibrosis patients. *Mol Microbiol* 70:1540–1555.
18. Xu CP, et al. (2008) *Staphylococcus aureus*-fibronectin interactions with and without fibronectin-binding proteins and their role in adhesion and desorption. *Appl Environ Microbiol* 74:7522–7528.
19. Coldren FM, et al. (2009) Encapsulated *Staphylococcus aureus* strains vary in adhesiveness assessed by atomic force microscopy. *J Biomed Mater Res A* 89:402–410.
20. Buck AW, et al. (2010) Bonds between fibronectin and fibronectin-binding proteins on *Staphylococcus aureus* and *Lactococcus lactis*. *Langmuir* 26:10764–10770.
21. Bustanji Y, et al. (2003) Dynamics of the interaction between a fibronectin molecule and a living bacterium under mechanical force. *Proc Natl Acad Sci USA* 100: 13292–13297.
22. Meenan NAG, et al. (2007) The tandem beta-zipper model defines high affinity fibronectin-binding repeats within *Staphylococcus aureus* FnBPA. *J Biol Chem* 282: 25893–25902.
23. Bode LGM, et al. (2010) Preventing surgical-site infections in nasal carriers of *Staphylococcus aureus*. *N Engl J Med* 362:9–17.
24. Peacock SJ, Day NPJ, Thomas MG, Berendt AR, Foster TJ (2000) Clinical isolates of *Staphylococcus aureus* exhibit diversity in fnb genes and adhesion to human fibronectin. *J Infect* 41:23–31.
25. Shinji H, et al. (2011) Role of fibronectin-binding proteins A and B in in vitro cellular infections and in vivo septic infections by *Staphylococcus aureus*. *Infect Immun* 79: 2215–2223.
26. Signäs C, et al. (1989) Nucleotide sequence of the gene for a fibronectin-binding protein from *Staphylococcus aureus*: use of this peptide sequence in the synthesis of biologically active peptides. *Proc Natl Acad Sci USA* 86:699–703.
27. Cunningham BC, Wells JA (1993) Comparison of a structural and a functional epitope. *J Mol Biol* 234:554–563.
28. Clackson T, Wells JA (1995) A hot spot of binding energy in a hormone-receptor interface. *Science* 267:383–386.
29. Fröman G, Switalski LM, Speziale P, Höök M (1987) Isolation and characterization of a fibronectin receptor from *Staphylococcus aureus*. *J Biol Chem* 262:6564–6571.
30. Schwarz-Linek U, Höök M, Potts JR (2004) The molecular basis of fibronectin-mediated bacterial adherence to host cells. *Mol Microbiol* 52:631–641.
31. Fersht AR, et al. (1985) Hydrogen bonding and biological specificity analysed by protein engineering. *Nature* 314:235–238.
32. Fersht AR (1987) The hydrogen-bond in molecular recognition. *Trends Biochem Sci* 12: 301–304.
33. Lumb KJ, Kim PS (1995) A buried polar interaction imparts structural uniqueness in a designed heterodimeric coiled coil. *Biochemistry* 34:8642–8648.
34. Petrey D, Honig B (2000) Free energy determinants of tertiary structure and the evaluation of protein models. *Protein Sci* 9:2181–2191.
35. Steinberg IZ, Scheraga HA (1963) Entropy changes accompanying association reactions of proteins. *J Biol Chem* 238:172–181.
36. Ross PD, Subramanian S (1981) Thermodynamics of protein association reactions: forces contributing to stability. *Biochemistry* 20:3096–3102.
37. Lamers RP, Stinnett JW, Muthukrishnan G, Parkinson CL, Cole AM (2011) Evolutionary analyses of *Staphylococcus aureus* identify genetic relationships between nasal carriage and clinical isolates. *PLoS ONE* 6:e16426.
38. Wang A, et al.; International Collaboration on Endocarditis-Prospective Cohort Study Investigators (2007) Contemporary clinical profile and outcome of prosthetic valve endocarditis. *JAMA* 297:1354–1361.
39. Li JS, et al. (2000) Proposed modifications to the Duke criteria for the diagnosis of infective endocarditis. *Clin Infect Dis* 30:633–638.
40. Yongsunthon R, et al. (2007) Correlation between fundamental binding forces and clinical prognosis of *Staphylococcus aureus* infections of medical implants. *Langmuir* 23:2289–2292.
41. Ros R, et al. (1998) Antigen binding forces of individually addressed single-chain Fv antibody molecules. *Proc Natl Acad Sci USA* 95:7402–7405.
42. Chothia C, Lesk AM (1986) The relation between the divergence of sequence and structure in proteins. *EMBO J* 5:823–826.
43. Guex N, Peitsch MC (1997) SWISS-MODEL and the Swiss-PdbViewer: an environment for comparative protein modeling. *Electrophoresis* 18:2714–2723.
44. Rostkowski M, Olsson MHM, Sondergaard CR, Jensen JH (2011) Graphical analysis of pH-dependent properties of proteins predicted using PROPKA. *BMC Struct Biol*, 10.1186/1472-6807-11-6.
45. Berendsen HJC, Postma JPM, van Gunsteren WF, Hermans J (1981) *Intermolecular Forces*, ed Pullman, B (D. Reidel Publishing Company, Dordrecht, Holland), pp 331–342.
46. Hess B, Kutzner C, van der Spoel D, Lindahl E (2008) GROMACS 4: Algorithms for highly efficient, load-balanced, and scalable molecular simulation. *J Chem Theory Comput* 4:435–447.
47. Frenkel D, Smit B (2002) *Understanding Molecular Simulation* (Academic, San Diego), 2nd Ed, p 638.
48. Parrinello M, Rahman A (1981) Polymorphic transitions in single-crystals: A new molecular-dynamics method. *J Appl Phys* 52:7182–7190.
49. Essmann U, et al. (1995) A smooth particle mesh Ewald method. *J Chem Phys* 103: 8577–8593.
50. Mosher DF, Proctor RA (1980) Binding and factor XIIIa-mediated cross-linking of a 27-kilodalton fragment of fibronectin to *Staphylococcus aureus*. *Science* 209:927–929.
51. Lower SK, et al. (2010) A tactile response in *Staphylococcus aureus*. *Biophys J* 99: 2803–2811.

Supporting Information

Lower et al. 10.1073/pnas.1109071108

SI Materials and Methods

Source of *Staphylococcus aureus* Isolates Used in Experiments. The Duke University Institutional Review Board approved this investigation. Bacterial isolates from infected cardiac device (CDI) and uninfected cardiac device (CDU) groups came from the *S. aureus* bacteremia (SAB) registry at Duke University Medical Center. The SAB registry has prospectively collected clinical data (initial admission and 12-wk follow-up) and the corresponding *S. aureus* isolate from each consenting adult inpatient with pure SAB at Duke University since 1994 ($n > 2{,}000$). Nasal carriage isolates were obtained from the anterior nares of healthy subjects (HS) living in the same geographic area as individuals infected with the disease-causing isolates.

Atomic Force Microscopy Experiments on Clinical Isolates of *S. aureus*. *S. aureus* isolates were cultured under conditions that promote the expression of fibronectin (Fn)-binding protein A (FnBPA) on the exterior surface of the cells (1, 2). Briefly, each growth culture was started from a cryogenically preserved sample. Each isolate was cultured to early exponential stage ($OD_{600} = 0.51 \pm 0.01$; $OD_{550} = 0.54 \pm 0.01$) at 37 °C in tryptic soy broth containing 0.25% dextrose. Growth curves were determined for 25 randomly selected clinical isolates to ensure similar growth characteristics for all isolates (i.e., the absorbance at early exponential stage). Approximately 1 mL of cell suspension was harvested using a centrifuge ($5{,}000 \times g$ for 3 min). Cells then were washed three times in saline solution. A small volume of washed cells (80 μL) was dropped onto an Fn-coated coverslip (BD Biosciences) and allowed to sit (without drying) for ∼5 min. Each sample was rinsed with PBS (pH 7.4) and placed in the atomic force microscope where force measurements commenced immediately.

The main text presents force measurements on individual cells from each of the 80 different clinical isolates described above. A Veeco/Digital Instruments Bioscope atomic force microscope and Nanoscope IV controller with an attached inverted microscope (Axiovert 200M; Zeiss) were used in these studies. The inverted microscope was used to locate and position the tip of the atomic force microscope tip over *S. aureus* cells. Silicon nitride probes [nominal tip radius 20 nm, measured spring constant 0.1 ± 0.06 nN nm^{-1} (3)] were used in these experiments. These probes were coated with Fn according to published protocol (2, 4). Some cantilevers were coated with BSA to characterize nonspecific interactions (5).

Forces were measured on cells immersed in PBS solution according to methods described in refs. 2, 4, and 6. Briefly, an Fn-coated probe was brought into contact with a bacterium and was pushed against the cell wall until the cantilever flexed 100 nm. The probe then was retracted away from the bacterium until the probe was separated completely from the cell. The vertical travel distance of the *z*-piezoelectric scanner was 2.7 μm. This process resulted in an approach force curve as well as a retraction force curve. A single approach–retraction cycle took 1–2 s (i.e., 0.5–1.0 Hz scan rate). Data acquisition was confined to ≤30 min from harvesting to assure cell viability (4).

Atomic force microscopy also was performed on an additional 16 isolates from the CDI ($n = 9$), CDU ($n = 1$), and HS ($n = 6$) groups. However, these isolates were excluded from the article because we did not have *fnbA* sequence data or multilocus sequence typing (MLST) information for these 16 isolates. It is important to note that our conclusions are the same when we include these 16 isolates. Specifically, the binding force and energy are both statistically stronger for the CDI isolates ($P < 0.01$) when $n = 96$ isolates (Fig. S3).

Molecular Dynamics Simulations of Fn Interactions with FnBPA. Molecular dynamics simulations were performed by starting with coordinates for Fn–FnBPA complexes determined by X-ray crystallography (7). The $^{4-5}$F1:FnBPA-5 complex [Protein Data Bank (PDB) ID code 2RL0] was used for the simulations of FnBPA-5 containing either D or E at position 652. The FnBPA-9 3D structure was obtained by replacement of the FnBPA-5 sequence in the Fn–FnBPA-5 complex ($^{2-3}$F1:FnBPA-5; PDB ID code 3CAL) and was used as a starting point for the simulations of Fn–FnBPA-9 complexes with H782Q and/or K786N in FnBPA.

Residue replacement was carried out using the DeepView software (8). A side chain rotational search was performed to avoid steric hindrance upon each replacement. His (H) and Lys (K) are both polar residues. Although Lys is positively charged at physiological pH, His can assume either a neutral or positive charge depending on its chemical environment. Gln (Q) and Asn (N) are both polar and generally uncharged amino acids. pK_a calculations were performed using the PROPKA program (9) to evaluate the protonation states of each titratable residue in the complex. No unusual protonation states were predicted. All histidines were predicted to be neutral and were treated as such.

The systems were solvated in explicit water using the simple point charge (SPC) water model (10), counter ions were added as necessary to ensure system neutrality, and geometry was optimized using 1,000 steps of the steepest descent algorithm. For each system, a 10-ns molecular dynamics simulation was performed. The simulations were conducted at the isothermal isobaric (NPT; N, moles; P, pressure; T, temperature) ensemble. Temperature was kept at 300 K using the Nosé–Hoover thermostat (11) with separate 1-ps relaxation times for solute and solvent. Pressure was maintained at 1 bar using the Parrinello–Rahman method (12) with the isothermal compressibility of 4.5×10^{-5} (kJ mol^{-1} nm^{-3})$^{-1}$ and relaxation time of 1 ps. A time step of 2 fs was used to integrate the equations of motion using the leapfrog algorithm (13). Periodic boundary conditions were used with a 1.4-nm cutoff for the nonbonded interactions. Long-range electrostatic corrections were taken into account by using the particle mesh Ewald method (14). The LINCS algorithm (15) was applied to all chemical bond lengths involving hydrogen atoms. Positional restraints were used on the C_α atoms using a force constant of 1,000 kJ mol^{-1} to avoid artificial repulsion between Fn and FnBPA caused by sequence replacement/molecular modeling and because the X-ray coordinates comprise only part of the full complex. This procedure ensured proper structural relaxation of the modeled side chains of receptor and ligand. Structural data were collected and analyzed at 500-fs intervals. All simulations were performed using the double-precision parallel version of the GROMACS 4 (16) in conjunction with the 53A6 parameter set of the GROMOS force field (17–19).

Atomic Force Microscopy Experiments on Peptides. Three synthetic peptides (>95% purity) were used in these experiments: (*i*) a 20-mer peptide whose sequence was identical to the native sequence of amino acids within *S. aureus* FnBR-9; (*ii*) a peptide with a single-residue change to mimic the polymorphism H782Q in FnBPA; (*iii*) a peptide with two residue changes to mimic H782Q and K786N in FnBPA. Gold-coated atomic force microscope tips were incubated in a solution of each peptide (100 μg L^{-1} in PBS) for 2 h. This incubation allowed direct linkage of each peptide to the atomic force microscope tip through a strong, covalent bond be-

tween the gold on the tip and the thiol group of the cysteine engineered at the C terminus of each peptide (20, 21). Two different peptide-functionalized tips were created for each of the three peptides. Measurements were performed in PBS on Fn-coated slides. Control experiments were performed with uncoated atomic force microscope tips on Fn-coated slides in PBS.

MLST and PCR of Adhesin Genes in the *S. aureus* Isolates. *S. aureus* genomic DNA was extracted using an ultraclean microbial DNA kit (MO BIO) in accordance with the manufacturer's instructions. MLST was performed as described previously (22). PCR assays were used to screen the *S. aureus* genome for 10 adhesion and/or biofilm-related genes, including bone sialoprotein-binding protein (*bbp*), clumping factor A (*clfA*), clumping factor B (*clfB*), collagen-binding adhesion (*cna*), elastin-binding protein (*ebpS*), extracellular fibrinogen-binding protein (*efb*), polysaccharide intercellular adhesin (*icaA*), and major histocompatibility analog protein/extracellular adherence protein (*map*/*eap*). The primers and conditions used to amplify the genes of interest are given in Table S5 (23).

Quantitative Real-Time RT-PCR Analysis of Expression of *fnbA*. *S. aureus* isolates were cultured to midexponential phase in tryptic soy broth at 37 °C. The cells were pelleted by centrifugation, resuspended in RLT buffer (Qiagen), and total RNA was isolated using the RNeasy kit (Qiagen) and Mini-BeadbeaterTM (Bio Spec Products) as described previously (24). Contaminating DNA was digested with DNase I (Ambion) for 1 h at 37 °, and 2 μg of RNA was converted to cDNA using the iScript One-Step RT-PCR kit (BioRad) according to the manufacturer's instructions. The reaction without reverse transcriptase enzyme was used as a control. Real-time RT-PCR reactions contained 2 μL cDNA or diluted no-RT control, 1 pmol forward and reverse primers, 8.5 μL nuclease-free deionized water, and 12.5 μL IQ SYBR Green Supermix (BioRad). Real-time RT-PCR was performed using an iCycler Real-Time PCR Detection system (BioRad) under the following conditions: 95 °C for 5 min, 40 cycles of 95 °C for 30 s, 55 °C for 30 s, 72 °C for 30 s. The normalized amount of transcript for each gene was expressed as the *n*-fold difference relative to the control gene ($2^{\Delta CT}$, where ΔCT represents the difference in threshold cycle between the target gene and the 16S rRNA gene). Samples were performed in triplicate, and each experiment was repeated three times to ensure reproducibility.

Adhesion Assay with 96-Well Plates. The adhesion assay with 96-well plates was modified from Peacock et al. (25). Briefly, 96-well plates were coated with 0.02% sodium carbonate (pH 9.6) containing Fn (10 μg/μL) overnight at 4 °C. The plates were washed with PBS, blocked with 2% BSA solution for 1 h at 37 °C, and then washed again. Bacteria were collected from broth cultures, adjusted to optical density 1.0 at 600 nm (corresponding to 10^7cells/mL), and incubated in the wells for 2 h at 37 °C. After washing with PBS, bacteria were fixed with 25% formaldehyde for 10 min, followed by the addition of 0.5% crystal violet for 1 min, and finally 100 μL DMSO. Absorbance was measured at 620 nm using a Multiskan Ascent plate reader (MTX Lab Systems). Absorbance values were expressed as a percentage of that recorded for *S. aureus* 8325–4 on the same plate.

1. Lowy FD (1998) *Staphylococcus aureus* infections. *N Engl J Med* 339:520–532.
2. Buck AW, et al. (2010) Bonds between fibronectin and fibronectin-binding proteins on *Staphylococcus aureus* and *Lactococcus lactis*. *Langmuir* 26:10764–10770.
3. Tortonese M, Kirk M (1997) Characterization of application specific probes for SPMs. *Proc Soc Photo Instrument Eng* 3009:53–60.
4. Yongsunthon R, et al. (2007) Correlation between fundamental binding forces and clinical prognosis of *Staphylococcus aureus* infections of medical implants. *Langmuir* 23:2289–2292.
5. Hanley W, et al. (2003) Single molecule characterization of P-selectin/ligand binding. *J Biol Chem* 278:10556–10561.
6. Lower SK, et al. (2010) A tactile response in *Staphylococcus aureus*. *Biophys J* 99:2803–2811.
7. Bingham RJ, et al. (2008) Crystal structures of fibronectin-binding sites from *Staphylococcus aureus* FnBPA in complex with fibronectin domains. *Proc Natl Acad Sci USA* 105:12254–12258.
8. Guex N, Peitsch MC (1997) SWISS-MODEL and the Swiss-PdbViewer: An environment for comparative protein modeling. *Electrophoresis* 18:2714–2723.
9. Rostkowski M, Olsson MHM, Sondergaard CR, Jensen JH (2011) Graphical analysis of pH-dependent properties of proteins predicted using PROPKA. *BMC Struct Biol*, 10.1186/1472-6807-11-6.
10. Berendsen HJC, Postma JPM, van Gunsteren WF, Hermans J, eds (1981) *Interaction Models for Water in Relation to Protein Hydration* (D. Reidel Publishing Company, Dordrecht, Holland), pp 331–342.
11. Frenkel D, Smit B (2002) *Understanding Molecular Simulation* (Academic, San Diego), 2nd Ed, p 638.
12. Parrinello M, Rahman A (1981) Polymorphic transitions in single-crystals: A new molecular-dynamics method. *J Appl Phys* 52:7182–7190.
13. Hochney RW, ed (1970) *The Potential Calculation and Some Applications* (Academic, New York), Vol 9, pp 135–211.
14. Essmann U, et al. (1995) A smooth particle mesh Ewald method. *J Chem Phys* 103: 8577–8593.
15. Hess B (2008) P-LINCS: A parallel linear constraint solver for molecular simulation. *J Chem Theory Comput* 4:116–122.
16. Hess B, Kutzner C, van der Spoel D, Lindahl E (2008) GROMACS 4: Algorithms for highly efficient, load-balanced, and scalable molecular simulation. *J Chem Theory Comput* 4:435–447.
17. Chandrasekhar I, et al. (2003) A consistent potential energy parameter set for lipids: Dipalmitoylphosphatidylcholine as a benchmark of the GROMOS96 45A3 force field. *Eur Biophys J* 32:67–77.
18. Lins RD, Hünenberger PH (2005) A new GROMOS force field for hexopyranose-based carbohydrates. *J Comput Chem* 26:1400–1412.
19. Soares TA, et al. (2005) An improved nucleic acid parameter set for the GROMOS force field. *J Comput Chem* 26:725–737.
20. Wagner P, Kernen P, Hegner M, Ungewickell E, Semenza G (1994) Covalent anchoring of proteins onto gold-directed NHS-terminated self-assembled monolayers in aqueous buffers: SFM images of clathrin cages and triskelia. *FEBS Lett* 356:267–271.
21. Ros R, et al. (1998) Antigen binding forces of individually addressed single-chain Fv antibody molecules. *Proc Natl Acad Sci USA* 95:7402–7405.
22. Enright MC, Day NPJ, Davies CE, Peacock SJ, Spratt BG (2000) Multilocus sequence typing for characterization of methicillin-resistant and methicillin-susceptible clones of Staphylococcus aureus. *J Clin Microbiol* 38:1008–1015.
23. Campbell SJ, et al. (2008) Genotypic characteristics of *Staphylococcus aureus* isolates from a multinational trial of complicated skin and skin structure infections. *J Clin Microbiol* 46:678–684.
24. Sharma-Kuinkel BK, et al. (2009) The *Staphylococcus aureus* LytSR two-component regulatory system affects biofilm formation. *J Bacteriol* 191:4767–4775.
25. Peacock SJ, Day NPJ, Thomas MG, Berendt AR, Foster TJ (2000) Clinical isolates of *Staphylococcus aureus* exhibit diversity in fnb genes and adhesion to human fibronectin. *J Infect* 41:23–31.

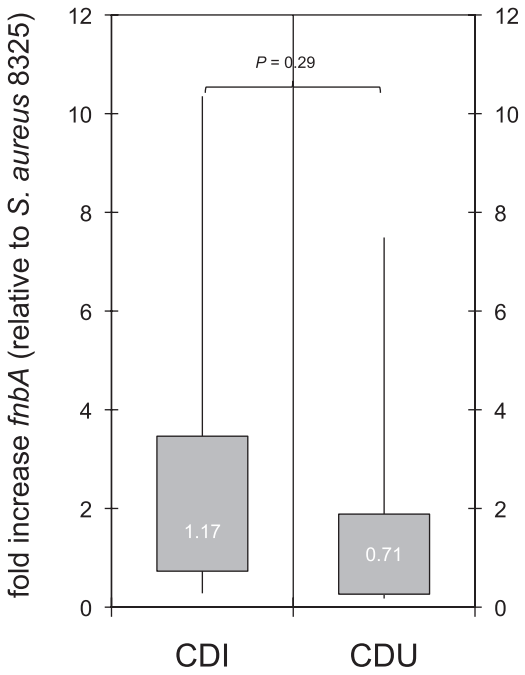

Fig. S1. Quantitative real-time PCR of *fnbA* expression in *S. aureus* isolates from the CDI (n = 26) and CDU (n = 20) groups. Box plot shows relative fold difference in *fnbA* expression compared with reference strain 8325–4. The t test was used to calculate P value.

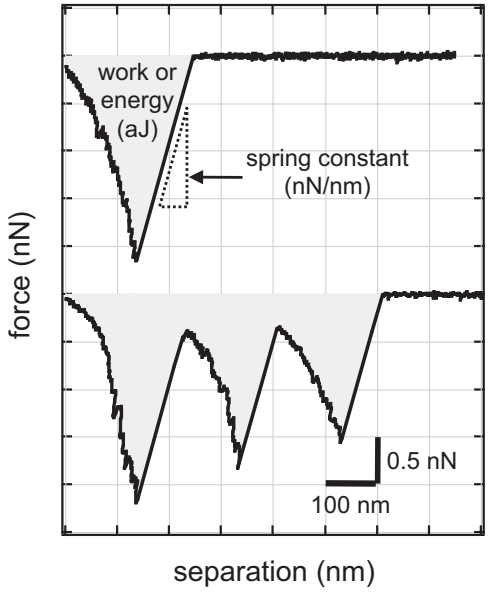

Fig. S2. Two retraction profiles measured when an Fn-coated tip was pulled from contact with a *S. aureus* bacterium expressing Fn-binding proteins. The work or energy of binding, in aJ (nN × nm), was determined by integrating each retraction force profile. Each rupture event terminates with a "jump from contact" line whose slope is equal to the cantilever spring constant. This feature occurs when the cantilever spring constant exceeds the actual force gradient between the tip and sample, causing the tip to snap free of the sample. A nearly vertical jump-from-contact line could be obtained with very stiff cantilevers, but such levers lack the sensitivity to measure small forces like those for biological samples. The area of integration may overestimate the work of binding because it incorporates the jump-from-contact event. However, any bias is the same for all *S. aureus* isolates, because all cantilevers used in this study were of the same type (long, narrow) and from the same wafer.

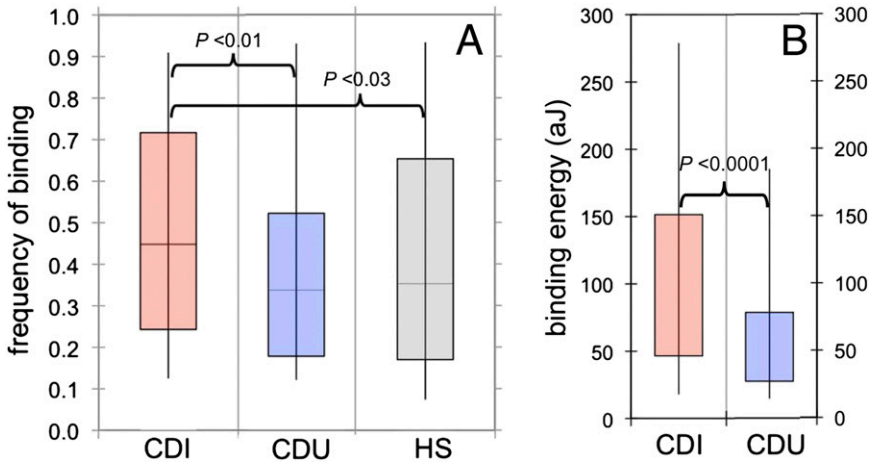

Fig. S3. Box and whisker plots of (*A*) frequency of observing a sawtooth force signature from CDI (n = 35), CDU (n = 21), and HS (n = 40) groups and (*B*) binding energy for *S. aureus* isolates from CDI (n = 35) and CDU (n = 21) groups. Whisker ends represent ninth and 91st percentiles. Data for 80 of these isolates are provided in the main text. The additional 16 isolates were excluded from the article because these isolates were analyzed only with atomic force microscopy. For these 16, we do not have the other data (e.g., *fnbA* sequence, MLST data, and/or presence/absence of MSCRAMM adhesin genes) that we obtained for the 80 isolates presented in the main text.

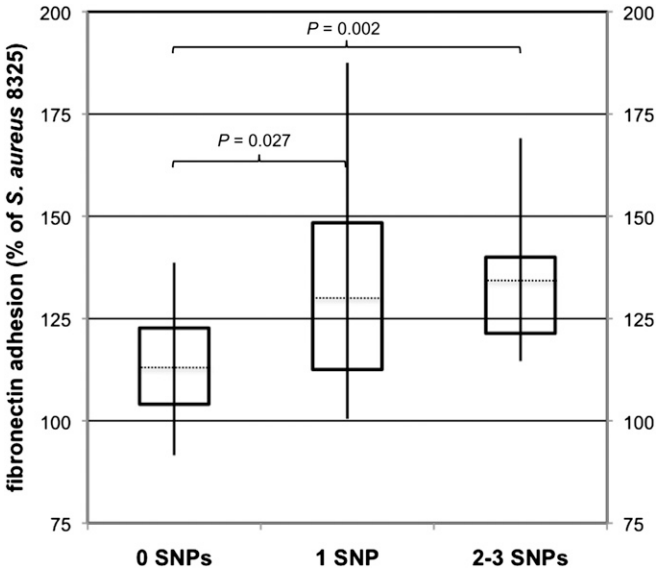

Fig. S4. Box plots of the Fn adhesion of clinical *S. aureus* isolates from CDU and CDI groups (n = 46) with none, one, or more than one of the following polymorphisms in FnBPA: E652D, H782Q, or K786N. Data are expressed as percentage of the mean adherence relative to the reference strain *S. aureus* 8325–4. The *t* test was used to calculate *P* values.

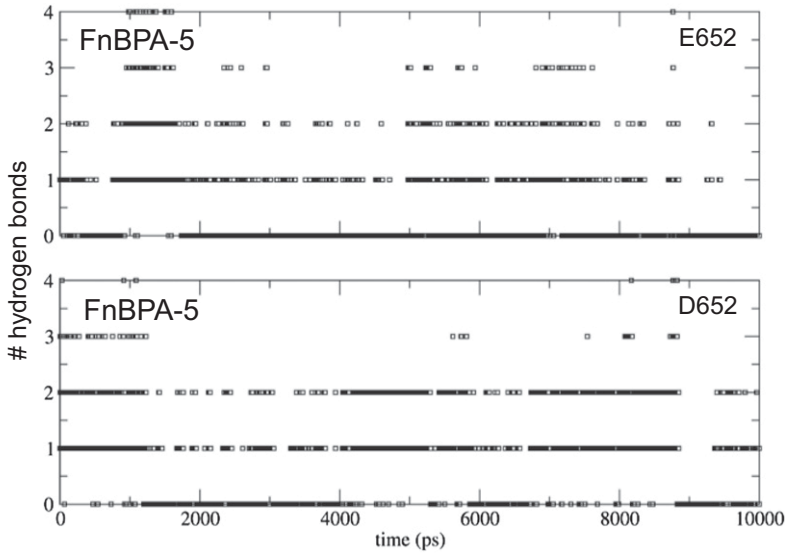

Fig. S5. Occurrence of hydrogen bonds between Fn and E652D in FnBPA-5. The average number of hydrogen bonds is 0.35 and 0.75 for FnBPA-5 sequences containing E652 and D652, respectively. Over the course of the simulation, the carboxyl group of E652 in FnBPA forms hydrogen bonds with the side chain of residues Ser-189 and Arg-191 in Fn in 27% of the sampled period; D652 forms hydrogen bonds with Fn 62% of the time.

Table S1. Demographic characteristics of persons who provided *S. aureus* isolates from infected cardiac devices (CDI), uninfected devices (CDU), or the anterior nares of healthy subjects (HS)

Characteristics	CDI (n = 26)	CDU (n = 20)	HS (n = 34)
Mean age in y (age range for HS)	60 ± 15	71 ± 11	10–29*
Race: % white (number)	85 (22)	75 (15)	71 (24)
Sex: % male (number)	62 (16)	55 (11)	68 (23)
% Methicillin-resistant *S. aureus* infection (number)	38 (10)	40 (8)	3 (1)
% hemodialysis dependent (number)	19 (5)	15 (3)	0[†]
% diabetes mellitus (number)	50 (13)	55 (11)	0[†]
% cancer (number)	8 (2)	10 (2)	n.d.[‡]
% late implantation[§] (number)	73 (19)	70 (14)	0
Device type[¶]			
Prosthetic valve	38 (10)	35 (7)	0
Permanent pacemaker or defibrillator	69 (18)	65 (13)	0

*94% of healthy subjects were age 10–29 y (20.6%age 10–19 y, 73.5%age 20–29 y).
[†]Hemodialysis and diabetes status was not recorded for one HS subject.
[‡]Not determined for HS subjects.
[§]More than 1 y.
[¶]Two patients had more than one device.

Table S2. Occurrence of polymorphisms E652D, H782Q, and K786N in FnBPA in *S. aureus* isolates from the patients with infected (CDI) or uninfected (CDU) cardiac devices and in isolates from anterior nares of healthy subjects (HS)

No. polymorphisms at positions 652, 782, 786 in FnBPA*	CDI (n = 26)	CDU (n = 20)	HS (n = 34)
0	23% (6)	80% (16)	59% (20)
1	19% (5)	15% (3)	27% (9)
2	42% (11)	5% (1)	15% (5)
3	15% (4)	0	0

*The occurrence of at least one of these polymorphisms was significantly more common in *S. aureus* from the CDI group than in the CDU (P = 0.0001) or HS (P = 0.0056) group. The occurrence of multiple (two or three) polymorphisms also was significantly more common in *S. aureus* from the CDI group than from the CDU group (P = 0.0002) or HS group (P = 0.0005). P values were calculated with the χ^2 test.

Table S3. Ancestral lineage and diversity of *S. aureus* isolates from CDI (*n* = 26), CDU (*n* = 20), and HS (*n* = 34) groups

	% (occurrence)			*P* value*	
Major clonal complex (CC)	CDI (n = 26)	CDU (n = 20)	HS (n = 34[†])	CDI vs. CDU	CDU vs. HS
CC5	19% (5)	15% (3)	0	1.00	0.0516
CC15	12% (3)	10% (2)	3% (1)	1.00	0.55
CC30	15% (4)	25% (5)	25% (8)	0.47	1.00
Other[‡]	54% (14)	50% (10)	72% (23)	1.00	0.14
Simpson's Index of Diversity	0.92	0.91	0.89		

Clonal relationships were determined by MLST analyses (1), and diversity was measured as the Simpson's Index of Diversity (2). Reported are the percentages (and number) of isolates for each major clonal complex (CC). The difference between groups was tested using a Fisher's exact test for CDI vs. CDU and for comparison of the two control groups (i.e., CDU vs. HS).

*Calculated with Fisher's exact test.

[†]MLST could not be performed successfully on two isolates from HS group.

[‡]Other category includes CCs with too few observations to test separately and isolates without an identified CC. For CDI these isolates included one CC1 isolate, one CC8 isolate, two CC20 isolates, and 10 isolates without identified CCs. For CDU these isolates included one CC1 isolate, one CC8 isolate, two CC45 isolates, one CC97 isolate, and five isolates without identified CCs. For HS these isolates included three CC59 isolates and 20 isolates without identified CCs.

1. Enright MC, Day NPJ, Davies CE, Peacock SJ, Spratt BG (2000) Multilocus sequence typing for characterization of methicillin-resistant and methicillin-susceptible clones of Staphylococcus aureus. *J Clin Microbiol* 38:1008–1015.
2. Hunter PR, Gaston MA (1988) Numerical index of the discriminatory ability of typing systems: an application of Simpson's index of diversity. *J Clin Microbiol* 26:2465–2466.

Table S4. Genotypic characteristics of *S. aureus* isolates for 10 adhesins (e.g., microbial-surface components recognizing adhesive matrix molecules; MSCRAMMs) associated with infection

	% (occurrence)		
Adhesion gene*	CDI *n* = 26	CDU *n* = 20	*P* value[†]
bbp; bone sialoprotein-binding protein	96 (25)	90 (18)	0.40
clfA; clumping factor A	100 (26)	100 (20)	NA
clfB; clumping factor B	100 (26)	100 (20)	NA
cna; collagen-binding adhesion	35 (10)	55 (11)	0.26
ebpS; elastin-binding protein	88 (23)	90 (18)	0.87
efb; extracellular fibrinogen-binding protein	100 (26)	95 (19)	0.25
icaA; polysaccharide intercellular adhesin	96 (25)	90 (18)	0.40
fnbA; Fn-binding protein A	100 (26)	100 (20)	NA
fnbB; Fn-binding protein B	85 (22)	100 (20)	0.0664
map/eap; major histocompatibility analog protein/extracellular adherence protein	96 (25)	100 (20)	0.38

Reported are the percentage (and number) of isolates with a particular adhesin gene from patients with infected (CDI; *n* = 26) or uninfected (CDU; *n* = 20) cardiac devices. Note the percent occurrence for the two Fn-binding proteins (*fnbA* and *fnbB*). All isolates possess *fnbA*. Although 100% of CDU isolates have *fnbB*, only 85% of CDI possess this adhesin gene.

*The primers and conditions used to amplify these 10 genes are described in ref. 1.

[†]Calculated with the χ^2 test.

1. Campbell SJ, et al. (2008) Genotypic characteristics of *Staphylococcus aureus* isolates from a multinational trial of complicated skin and skin structure infections. *J Clin Microbiol* 46: 678–684.

Table S5. Sequences of template and sequencing primers for Fn-binding regions of *fnbA*

Primer	Sequence
Forward	
fnbA-F	5′-CCGAACAATATAGACTTGCATTTATT-3′
fnbA-F1	5′-GAACACAAATGGTAGGACATCCAGAGCAAC-3′
fnbA-F2	5′-CAATAGAAGAAACGGATTCATCAGCTATTG-3′
fnbA-F3	5′-CTGGTTTAGGAACTGAAAATGGTCACG-3′
fnbA-F4	5′-CAGTCATTCGAGGAAGATACAGAAAAAGAC-3′
Reverse	
fnbA-R	5′-CATCAGACATAAACCAATGAAGCAATCAG-3′
fnbA-R1	5′-CTTCATATTCAACAACATCAGCGTGATG-3′
fnbA-R2	5′-CCCGTGACCATTTTCAGTTCCTAAACC-3′
fnbA-R3	5′-GTTGTATCTTCAATCGTTTGTTGACCTTC-3′
fnbA-R4	5′-CTTTACCTTGTTCCACTGGTTTAGAAGG-3′

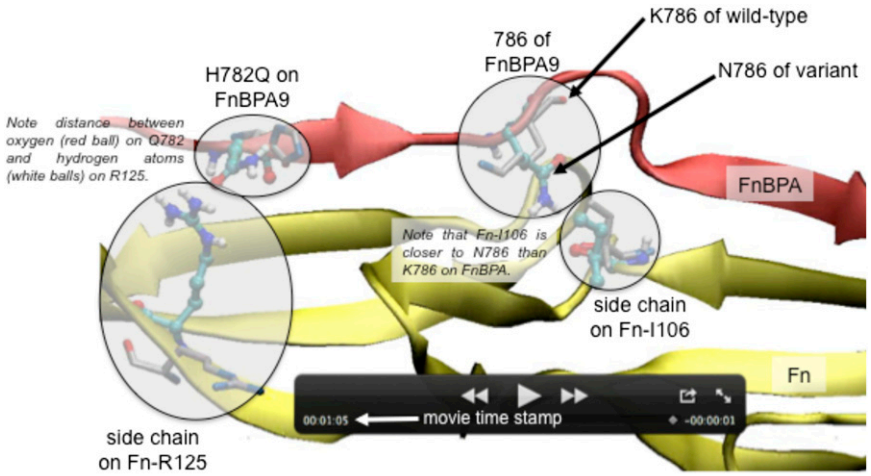

Screen grab of MD simulation of Fn-Fn
stick model – simulations for Fn and wild Fn
CPK model – simulations for Fn and variant Fn

Movie S1. The movie shows the last 5 ns of the simulations for the Fn–FnBPA9 complexes. Fn (yellow) and FnBPA9 (red) are displayed in the cartoon, where the arrows represent β-strands. The side chains of the pairs Q782/R125 and N786/I106 in the double SNPs are shown in the Corey–Pauling–Koltun (CPK) model (carbon, cyan; oxygen, red; nitrogen, blue; hydrogen, white). The side chain of the corresponding pairs in the FnBPA9 wild-type (H782/R125 and K786/I106) is shown in the stick model (carbon, gray; oxygen, red; nitrogen, blue; hydrogen was omitted for clarity). As can be seen from the relative distance between the pairs Q782/R125 and N786/I106 in the double-SNP sequence, an electrostatic interaction (hydrogen bond) is formed. This interaction is clearly absent in the Fn–FnBPA9 wild-type complex. This movie was created with VMD 1.8 software (Visual Molecular Dynamics) (1).

Movie S1

1. Humphrey W, Dalke A, Schulten K (1996) VMD: Visual molecular dynamics. *J Mol Graph* 14:33–38, 27–28.

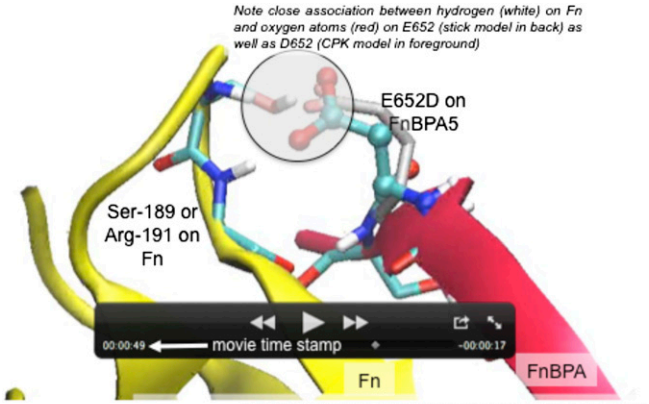

Screen grab of MD simulation of Fn-FnBPA5
stick model – simulations for Fn and wild FnBPA5
CPK model – simulations for Fn and variant FnBPA5

Movie S2. The movie shows the last 5 ns of simulation comparing FnBPA5 652E and 652D. As in Movie S1, Fn (yellow) and FnBPA5 (red) are represented in the cartoon, where arrows represent β-strands. Residue 652D (SNP variant) is shown in the CPK model (carbon, cyan; oxygen, red; nitrogen, blue; hydrogen, white). Residue 652E (wild-type) is shown in the stick model (carbon, gray; oxygen, red; nitrogen, blue). Following the latter color code, residues on Fn turn on and off as they form hydrogen bonds with the carboxyl groups of the residues at position 652. Only polar hydrogens are displayed. Visual inspection clearly shows that D562 has a higher affinity to Fn than does E652. The reason is likely higher entropy because of the longer side chain of the glutamic acid as well as its greater exposure to the solvent. This movie was created with VMD 1.8 software (1).

Movie S2

1. Humphrey W, Dalke A, Schulten K (1996) VMD: Visual molecular dynamics. *J Mol Graph* 14:33–38, 27–28.